Comparing Oxidation of Aluminum by Oxygen and Ozone Using Reactive Force Field Molecular Dynamics Simulations

Fateme Saidinik
University of Tehran
Hassan Behnejad (behnejad@khayam.ut.ac.ir)
University of Tehran

Research Article

Keywords: Aluminum, ozone, oxidation rate, molecular dynamics simulation, ReaxFF, amorphous, oxide layer

Posted Date: April 15th, 2022

DOI: https://doi.org/10.21203/rs.3.rs-1550460/v1

Additional Declarations: No competing interests reported.

Abstract

This work investigated the Al(100) surface oxidation simulations by O_2 and O_3 molecules at 400, 600, and 800 K temperatures with the Reactive Force Field (ReaxFF) method. One hundred ozone molecules and 150 oxygen molecules were placed in an empty space above the Al(100) surfaces in separate simulation boxes to compare this metal's behavior with them (gases incipient density of 0.47 g/cm^3). We found further growth of the oxide layer in the case of ozone-aluminum. Subsequently, we surveyed the correlation between temperatures and the growth of alumina layers in the case of oxygen and ozone in separate sets through ReaxFF simulation to untangle the mechanism of oxidation kinetics of the Al(100) surface by ozone. Even though there are proven constraints on growing an oxide layer with ozone as well as oxygen, it’s possible to produce a thicker oxide layer at lower temperatures using ozone.

1. Introduction

Periodic table's 13th element, aluminum, is broadly used in energetic applications, functioning as plasmonics, nanofluids, explosives, solid propellants, and firefighting materials [1–4].

The widespread use of aluminum is due to its high combustion enthalpy, low toxicity, abundance, and good stability [5, 6].

A thin layer of oxide is automatically shaped on aluminum by placing it in any place, which produces an intricate amorphous structure during uncontrolled steps.

Researchers have been trying to understand and search for the steps of aluminum oxidation for many years. There are numerous experimental and theoretical studies investigating species and factors affecting the properties of the oxide layer and its quality.

Most studies on aluminum oxidation involve explaining the stages of thermal oxidation of aluminum in terms of temperature [7–9].

Aluminum oxide has developing applications as well as aluminum. For instance, thin aluminum-oxide films are employed in numerous microelectronic devices as a dielectric, diffusion, or tunneling barrier [10–12].

In order to optimize the application of aluminum-oxide films, it is required to consider layer thickness, morphology, physical and chemical properties [13].

Thus, researchers have done hundreds of theoretical and practical studies from micron-sized aluminum surfaces in older studies [14] to its nanoparticles [15, 16].

During these years, in addition to studying the structure of aluminum oxide and the factors affecting the morphology of the structure, the mechanism of this process has also received much attention [17–20].

These studies mainly aim to describe the successive stages of oxygen attachment to aluminum, oxide layer formation, and kinetics understanding is performed.

By increasing the oxidation temperature up to 1073 K, it has been reported [17] that approximately all the nanoparticles turn into hot solid spheres, and when reaching the temperature of 1373K, they are found to be hollow.

The oxidation steps could be explained in terms of temperature as follows: Aluminum is initially coated with a thin layer of amorphous oxide, which significantly reduces the oxidation rate. At temperatures > 873 K, the oxidation rate increases due to the conversion of the amorphous layer to a crystalline state. If the temperature increases up to 973 K, the oxidation rate decreases due to the destruction of the diffusion paths. The re-oxidation rate increases at temperatures above 1273 K because the molten aluminum protrudes out of the shell [21].

In fact, before the melting temperature, oxidation occurs through the diffusion of O_2 into the aluminum oxide shell, and above the melting point, aluminum and oxygen diffuse through the oxide shell to raise the oxidation rate [17].

Henz *et al.* studied the simulation of aluminum nanoparticles which were covered with an oxide layer by a thickness of 1 and 2 nm and showed oxidation inception occurs with the swift propagation of aluminum ions to the surface of the nanoparticles, and this was in agreement with the experimental endeavors that have beholden the formation of hollow [17–18].

Jeurgens and colleagues described a mechanism in the incipient Al oxidation that the oxide-film evolvement is finite at temperatures up to 573 K due to the low locomotion of the oxygen species. However, at higher temperatures, while the growth of the layer is not restricted, a phase transition "amorphous-to-gamma-Al_2O_3" occurs [22]. Chu *et al.* studied simulation of Core-Shell Al/Al_2O_3 nanoparticles in an oxygen atmosphere. In addition to presenting a 4-step mechanism, they noted that during the melting phase, aluminum atoms propagate out of core Al atoms, while in the fast oxidation stage, inward diffusion of shell O prevails [19].

Along with increasing studies and growing applications of aluminum and aluminum oxide, a group of researchers took an interest in the oxidation of substances with ozone. Since then, these researches have constantly been expanding [23–27].

Kuznetsova and colleagues oxidized aluminum via an ultra-high vacuum apparatus using previously produced ozone in a generator at a temperature of 300 K.

They showed that the average resistance for oxide layers produced with ozone was ~ 10 times higher than that of oxygen-oxidized layers. The oxidized layer using 97% pure ozone was also superior in terms of corrosion passivation compared to the oxygen-oxidized layer [28].

Silicones oxidation by ozone has been prevalent for many years. However, ozone production has sometimes been a problem [27 and 29]. Oxidation of silicones with ozone requires lower temperatures and exhibits the Si/SiO_2 interface with higher quality, but this entails further studies in the oxidation of metals. For instance, the effects of system temperature on the oxidation of metals by ozone have not been completely investigated.

On the other hand, when reviewing the published studies of the last decades, one would realize that there have been numerous experimental studies in metal oxidation from which notable conclusions have been drawn [30–33]. However, complexity, high laboratory costs, lack of reproducibility, and not providing a detailed explanation of the oxide layer formation in metal oxidation studies have caused a growing tendency towards molecular dynamics simulations.

Molecular simulation methods using empirical force fields have been widely employed in researching atomic systems up to 10,000 atoms simulation.

For instance, the embedded atom method and the modified one are precise in physical properties' calculations of various metals and alloys such as melting points, viscosities, elastic, and diffusivity constants [34–35]. The reactive force field (ReaxFF) method, originally developed by van Duin *et al.*, has been widely applied in simulations of different oxidation states of metal, reactive crosslinking of polymers, and oxidation and pyrolysis of hydrocarbon fuels [36–38].

ReaxFF utilizes empirically specified interatomic potentials inside a bond-order formalism. In this manner, it can model events that involve connecting or breaking chemical bonds without explicitly considering quantum mechanics (QM), which entails very high costs for large atomic systems [39].

The present study investigates the oxidation of aluminum with ozone and oxygen at different temperatures using ReaxFF molecular dynamics.

The main purpose of this work is to provide an accurate atomic-level insight into the study of oxide films formed in the thermal oxidation of aluminum (100) surface with oxygen and ozone molecules and to examine the effect of temperature on this oxidation.

The article proceeds in the following order to achieve this goal: First, we briefly explain the chosen reactive force field (ReaxFF) to examine Al/O interactions. Then we explore the incorporation of oxygen molecules into the surface of aluminum (100) in the three different temperatures 400, 600, and 800 K and elucidate the effect of temperature on metal oxidation with regard to earlier studies. In the next part of this study, we investigate the aluminum oxidation through ozone molecules in conditions similar to the oxidation of aluminum with oxygen. Finally, we present our results and findings on the oxide layers produced in simulated conditions.

2. Methods

2.1 Computational method

Due to a large number of particles in molecular systems, it is sometimes not possible to obtain the properties of systems by analysis.

Every day more and more, Molecular Dynamics (MD) methods are gaining value and importance in all fields such as chemistry, biomolecule cognition, physics, and mathematics. These methods gradually become a powerful tool for scrutinizing systems that are sometimes difficult or impossible to study experimentally.

In molecular dynamics, the interplay among particles is formulated with simplified mathematical functions.

two of the most admirable approaches in the last decades have been RMD and RXMD methods which simulate the formation or breaking of bonds during chemical reactions, and these methods can use one of the most advanced reactive force fields (ReaxFF), developed by van Duin *et al*. [38]

ReaxFF is an empirical reactive force field. It is most crucial discord with non-reactive force fields is that it notices and updates the electrical charges of species and changes the bond order according to the distance between atoms at each time step when converting reactants to products [40–41].

Despite its need for more robust and higher-cost technologies, this method maintains efficiency because it can simulate a large number of atoms or longer times.

Therefore, this potential has been inclusively used in some reactive systems due to enumerated advantages.

The total energy of the system in ReaxFF potential is formulated as Eq. (1):

$$E_{total} = E_{bond} + E_{over} + E_{lp} + E_{under} + E_{val} + E_{tors} + E_{vdWaals} + E_{Coulomb,} \quad (1)$$

where E_{total} is the total potential energy, E_{bond}, E_{over}, E_{lp}, E_{under}, E_{tors}, $E_{vdWaals}$, $E_{Coulomb}$ and E_{val} expose covalent bond, over coordination, lone-pair, under-coordination correction, torsion angel, van der Waals energy, Coulomb and valence angle, respectively [37].

ReaxFF is formulated based on a bond-order/bond-energy to manage changes in atom connectivity and uses a geometry-dependent outline called EEM (electronegativity equalization method) [42] to calculate the partial charge. Further details of this effective method can be found in the extensive studies of many authors [36–37 and 43].

2.2 Simulation setup

Based on what was described above, simulation studies of both sets of aluminum-oxygen and aluminum-ozone have been performed based on the Reactive Force Field (ReaxFF).

We exerted the same ReaxF parametrization, which was employed for Aluminum oxidation by Hong and van Duin, who had determined force field parameters by changing the temperature at two primary oxygen pressures on the oxide growth kinetics of aluminum nanoparticle (ANPs) [38].

All the simulations were executed by the open-source LAMMPS code [44].

Whereas to rummage the trajectory of molecular dynamics (MD) simulation platform, open visualization tool (OVITO) and Visual Molecular Dynamics (VMD) were used as visualization tools to provide the built-in analysis [45–46].

Since pure aluminum has a face-centered-cubic (fcc) crystal structure, this work initially attempted to design of fcc-Al crystal containing 576 Al(100) atoms and staked the slab in a simulation box with the approximate dimensions 16.2 × 12.1 × 48.5 $Å^3$, then at the top and bottom of the box, along the z-axis, vacuum layers with dimensions of 25 Å were added.

Described simulation box was designed in two sets (A and B) and was randomly dispensed in the vacuum of two sets consisting of 150 oxygen and 100 ozone molecules, respectively (gases incipient density of 0.47 g/cm^3) were prepared to perform simulations at 400, 600, and 800K temperatures according to Figs. 1(a), 1(b), 1(c).

In this work, the Nose-Hoover thermostat was used to retain goal temperature, and all simulations were implemented using canonical ensemble (NVT). Additionally, as suggested by previous works, we applied periodic boundary conditions in all the principal directions to minimize related issues with boundary effects and finite-size [47–48].

Equilibration in Al-O_2 and Al-O_3 systems has been executed under NVT ensemble using Nose-Hoover thermostat with a damping parameter of 100 fs for 40 ps to omit any hot spots in the inceptive configuration and also minimize energy to eliminate simulation artifacts produced by collisions at high energies.

Then to obtain simulation trajectories, we enforced MD simulation for 200 ps using a time step of 0.2 fs & 1000000 iterations.

3. Discussion And Results

3.1 Radial Distribution Function Analysis

At first, to comprehend the mechanisms of atomic diffusion and assess the accuracy of the simulation results, we use radial distribution function analysis. RDF is one of the essential quantities for determining the structure of a system, which determines the positional structure and order of atoms relative to each other. In other words, $g\left(r\right)$ demonstrates the probability to observe atom B in a (dr) shell at the (r) distance of atom A, which is chosen as a basis or standard for evaluation and depends on the

temperature and density of the system; moreover, it can be found both experimentally and through simulation [49]. The neutron weighted radial distribution function is described by: [13]

$$g_N(r) = \frac{\sum_{\alpha\beta} c_\alpha b_\alpha c_\beta b_\beta g_{\alpha\beta}(r)}{\left[\sum_\alpha c_\alpha b_\alpha\right]^2}. \quad (2)$$

where r is the distance between a pair of particles, $g_{\alpha\beta}(r)$ is the partial pair distribution functions found at a distance r. Figures (2) shows the radial distribution functions of Al-Al, Al-O, and O-O. We extracted from the first peak in $g_{\mathrm{O-O}}$, $g_{\mathrm{Al-Al}}$, and $g_{\mathrm{Al-O}}$ at Figure (2) that for aluminum and oxygen at a temperature of 600K, the nearest -neighbor atomic distances O-O, Al-Al, and Al-O are 2.7, 3.1, and 1.74 Å, respectively. These results are in line with available studies on aluminum oxidation [50–52]. It should be noted that in some articles at low oxygen pressures in $g(r)$ for O-O there are small pre-peaks that are not seen due to the relatively high gas pressure of the present article [48].

In Fig. 2(e), in the amorphous structure of aluminum oxide, the existence of the first peak with long-height and the lack of subsequent peaks are substantial because of the lack of long-range order. While in the aluminum structure, the presence of several visible peaks shows a structured shape 2(a), 2(d).

When the temperature increases, the position of the Al-Al first peak changes trivially, while the decrease in the height of the first peak indicates that the order of the structure has decreased. However, similar changes by increasing the temperature in the first peak Al-O were not observed, which in our opinion shows the structured form of alumina.

Another perspective in this study is to compare the radial distribution function of aluminum-ozone to the same distribution function for aluminum-oxygen at 600 K.

In the same way, we obtained $g_{\mathrm{O-O}}$, $g_{\mathrm{Al-Al}}$, and $g_{\mathrm{Al-O}}$ for interactions among aluminum and ozone at the temperature of 600 K, and according to the first peak, the nearest-neighbor atomic distances for Al-Al, O-O, and Al-O were 3.11, 2.5, and 1.64 Å, respectively. (Figs. 3(a), 3(b), 3(c))

The position of the first peak of Al-Al, and its height does not have a significant shift, but the nearest neighbor in O-O is closer by 7.4%, and the peak height has increased by 11.11%.

The position of the first peak of Al-O is seen at a 5% closer distance, and the aluminum coordination number is probably larger than the same aluminum number in aluminum-oxygen interaction because we see an increase in the height of the first peak. The reduction of bond length Al-O in ozone molecules colliding with the surface of aluminum can indicate an increase in the density of the oxide layer composed of ozone and aluminum [53].

Additionally, in the temporal analysis of the radial distribution function, the first peak Al-O for Al/O_3 and Al/O_2 interaction is formed in 2.8 and 6 ps, respectively, which is a supplemental witness for the faster oxidation of ozone that the following sections have illustrated.

Furthermore, the average coordination number was computed by integrating around the first peak in the radial distribution function [48]:

$$CN_{\alpha\beta}(R) = \rho c_{\beta} \int_{0}^{R} g_{\alpha\beta}(r)\, 4\pi r^2 dr$$

3

where R or the cut-off radius propound, is generally considered as the distance to the first minimum of g (r), which was 3.7, 3.3, and 2.3 for Al-Al, O-O, and Al-O (Fig. 2), respectively, in the case of aluminum and oxygen at 600K, each aluminum atom is surrounded by 8.5 aluminum atoms and 4.2 oxygen atoms. In contrast, at the same temperature for ozone, each atom of aluminum is surrounded by 7.8 atoms of aluminum and 5.7 atoms of oxygen. It can be said that when aluminum is bombarded with ozone, oxygen atoms are able to penetrate more into aluminum-affluent rings.

3.2 Consumption amount of oxygen and ozone

One way to understand the reaction rate is to consider the ozone and oxygen consumption rate as a function of simulation time and its temperature dependence. Thus, we examined the oxygen and ozone consumption rate at three different temperatures for 200 ps according to the diagrams in Figs. 4(a), 4(b).

Once simulation starts, oxygen, and ozone molecules instantly turn into atoms, are absorbed on the aluminum surface (100), and begin to penetrate the lattice.

Notwithstanding the upward trend of oxygen and ozone consumption, the gradient of this ascent and its amount for different temperatures and oxidants appreciably varies, which is visualized in table (1).

Table 1
The number of oxygen atoms consumed in terms of simulation time at different temperatures.

Reactants		**$Al + O_2$**	**$Al + O_3$**
Temperature	Time	Oxygen atoms consumed	Oxygen atoms consumed
	t = 10ps	81	79
400K	t = 100ps	161	210
	t = 190ps	167	214
	t = 10ps	91	90
600K	t = 100ps	175	238
	t = 190ps	186	247
	t = 10ps	101	97
800K	t = 100ps	192	280
	t = 190ps	209	294

Examining Table 1, which is obtained from simulation calculations, we find that in 10 ps, the number of consumed atoms from the decomposition of ozone and oxygen is not much different. Therefore, it could be concluded that in the preliminary stages of oxidation, when there are numerous active levels of aluminum, the penetration of ozone or oxygen molecules into aluminum are not different. Over time, we can see a striking increase in the consumption of oxygen atoms in the aluminum-ozone system, explicitly at high temperatures. The consumption rate of ozone at temperatures of 400, 600, and 800K is 0.75, 0.87, and 1.09 atom/ps after the initial ten ps, respectively. The same amounts for oxygen are 0.47, 0.52, and 0.6 atom/ps, respectively, proving the significant amount of ozone consumption at higher temperatures. Based on these findings, it is probable that the ozone-produced oxide film is thicker. This has been confirmed in the next section as well as in experimental works [28].

Due to the difference in the slope of oxygen and ozone consumption, we believe that there are empty spaces on the aluminum surface that are attacked by oxygen or ozone. We will illustrate this mechanism according to other evidence in the following sections. On the other hand, considering the rate of oxygen and ozone consumption, it is clear that the active places on the surface of aluminum are covered with ozone more effectively. We measured the thickness of oxide film formed on the surface of aluminum by ozone and compared it with the thickness of the oxide layer produced by oxidation with oxygen in the next section.

3.3 The oxide film thickness and oxidation mechanism

We used the ReaxFF-MD simulation for aluminum interactions with different allotropes of oxygen by varying the temperature from 400 to 800 K in relatively high oxygen and ozone gas pressure to exhibit the

formation of the oxide film during simulation time.

Afterward, the thickness of the oxide layer at the aforementioned temperatures was computed for both ozone and oxygen. They are plotted in two ways to understand and probe the outcomes. Figure 5 aids in understanding the impression of temperature on oxide film thickness, and Fig. 7 indicates the growth of the oxidized layer at different temperatures to clarify the ozone and oxygen differences in oxidation aluminum.

The snapshots of the oxide film on Al(100) with ozone at 600 K and different times are shown in Figs. 6(a), (b), (c), (d), (e). Pursuant to foregone findings in experimental or simulation studies, ascending temperature causes the thickness of aluminum oxide layers to increase. Howbeit, Jeurgens *et al.* recorded an inverse relationship between temperatures greater than 673 K and layer thickness after a long period of oxidation.

(> 2500s), which is not achievable in MD techniques [22, 54–56]. In the case of aluminum interactions with oxygen, an increasing effect on the thickness of the oxide layer is observed at higher temperatures, according to Fig. 5. Interestingly enough, considering what could be envisaged from the plenty consumption of ozone molecules, the thickness of the oxide layer produced from it is greater. In our opinion, the higher oxidizing power of ozone causes more layers to oxidize than oxygen; nevertheless, this should be further investigated in future studies.

Our other prospect in this work is to survey the confined oxide layer grown on Al(100) at lower temperatures. In fact, aluminum nanoparticles make the oxide film at a quick rate by transferring high heat and mass at an incipient level, but the growth is quickly restricted. In the current study, we see that both oxidation and ozonation are limited at 400 K after 105 ps. According to our findings, at temperatures, less than 600 K, the consumption of oxygen molecules rises originally but then gets limited, which is probably due to the growth of an oxide layer on aluminum (100). At higher temperatures (> 600 K), the growth of the oxide layer is not restricted, which is in line with the simulation findings of van Duin *et al.* [38]. As visualized in Fig. 6, in the case of ozone molecules interactions, at 600 and 800 K, the growth of the oxide layer is not restricted, which is consistent with predominant experimental studies [28].

The layer thickness change in 40-ps intervals is submitted in Fig. 7. The average layer-growth rate attained at 600 K during the first 14 Å thickness for ozone was calculated to be ~ 0.11 Å/ps, achievable at 800 K for oxygen. It seems that ozone works as a more reactive oxidant because it probably decreases oxidation temperature, this has been previously reported in the oxidation of silicon with ozone by Kazor and Boyd [57]. Figure 7 refers to the differentiating results of ozone or oxygen interactions with aluminum. According to this Figure, the growth of each layer produced by ozone or oxygen in the final times periods is very low and confined at 400 K, but over a period of 160 to 200 ps, the oxide films grown by ozone are much less limited at 800 K.

Based on the above evidence, our proposed mechanism for the growth of the oxide layer produced by ozone is as follows: In step (I), the absorption of ozone molecules upon the Al(100) surface starts the

oxidation. While ions and electrons are transferring, the amorphous alumina is formed, which has higher thermodynamic stability than the crystalline state [22]. The aluminum atoms leave the sublayer, come up, and bond with the oxygen atoms. In non-stoichiometric clusters, the charge of the cations changes to Al^{2+} and Al^{4+} toward rectifying the stoichiometric defect. In our opinion, there is not much difference between ozone and oxygen at this stage. Noting that the first stage is accompanied by an increase in the number of Al-O bonds, which is completely visible in the diagrams of $g(r)$ in our study after a short time, while these bonds are surrounded by numerous Al-Al bonds in many rings full of aluminum atoms, which is consistent with existing findings [48–58].

Then at stage (II), when ozone molecules assail the hot nether surface and are decomposed to oxygen molecules, oxygen radicals, and probably O_3^- radicals, the oxidation rate is higher than that of simulation with pure oxygen molecules, according to the above evidence. In our opinion, the distinction in oxidation rate for ozone is related to the second stage, where ozone molecules create free radicals that cause surface oxidation to run more quickly. These free radicals have been reported by Lian *et al.* and Koike [27, 29], and their existence has been confirmed in the oxidation of silicon. Hence, the surface of aluminum is oxidized by oxygen, wherein a significant concentration of free radicals and oxygen atoms build an extra oxide layer while ion diffusion extends. It is as if a re-doping with oxygen atoms occurs, which we opine can lead to an increase in the thickness of the oxide layer.

The thermodynamic instability of ozone relative to oxygen, its ability to beget various radicals [59], as well as the greater electron-affinity of ozone relative to oxygen that is 1.46 and 2.10 eV, respectively, can be considered as reasons why ozone is acting in a particular way.

The third oxidation stage: A layer of amorphous aluminum oxide with a very hot internal temperature is now formed on the Al(100) surface. In perusals performed at high temperature (> 873 K) in this stage, amorphous crust remodels to a crystalline phase, which is not the subject of this study [38]. As mentioned in the previous sections, the O-O bonds for Al-ozone interaction are greater at the metal-oxide interface, and some of them are outside the oxide layer. This leads to an increase in free volume introduced by Trybula *et al.* [48]. In our belief, it aligns with the re-doping of oxygen atoms and radicals acting on oxidation by ozone and causes the oxide layer to continuously grow, especially at high temperatures. Figure 8 represents the oxide development in ozone.

3.4 Density, charge distribution

When understanding the growth mechanism of the oxide layer, the structure of the produced layer should also be determined. Indeed, the layer morphology and its effects on the diffusion of ions are effective in the layer growth rate. Considering the density of the layer produced by ozone and comparing it with the layer produced by oxygen in similar conditions, one can conclude that the higher density of the ozone produced layer is due to the increases outside the metal-gas interface in the stage (II) in O-O bonds, which reduces free spaces and increases the density of the layer; however, more research is being done.

The charge distribution of aluminum and oxygen atoms along the z-axis for the interactions of aluminum and ozone at a 600K temperature is shown in configuration 9. The entire charge of the oxide-layer is neutral, but near the surface of the oxide layer, oxygen atoms accede to negative charges ranging from − 1.9e to − 2.16e, and aluminum atoms attain positive charges ranging from + 2.1e to + 2.2e, which seems slightly higher than the ReaxFF method [60], and shall be another evidence for faster oxide layer formation by ozone.

4. Conclusions

Amidst procedures to raise the rate of Al_2O_3 formation, this article inquiries molecular dynamics simulations of aluminum oxidation with O_3 molecules and its discords with oxidation by oxygen at different temperatures, and inferred that the rate of ozone penetration into aluminum is higher and the density of the layer that is formed is higher. The effect of temperature on the growth of the oxide layer was inspected; not only do higher temperatures cause more layer growth, but also reduce the inherent limitation of layer formation due to the more empty spaces it creates. In addition, we described the mechanism of ozone oxidation, which we believe has three stages. Eventually, by comparing the charges of oxygen and aluminum atoms, deducted that the interaction of aluminum with ozone is more intense.

Declarations

Acknowledgment

We would like to express our sincere thanks to the Research Council of the University of Tehran for the financial support of this work.

References

1. G.H. Chan, J. Zhao, G.C. Schatz, R.P. Van Duyne, Localized Surface Plasmon Resonance Spectroscopy of Triangular Aluminum Nanoparticles, Journal Physical Chemistry **C112**, 2008 (13958).
2. R. Taylor, S. Coulombe, T. Otanicar, P. Phelan, A. Gunawan, W. Lv, G. Rosengarten, R. Prasher, and H. Tyagi. , Small particles, big impacts: A review of the diverse applications of nanofluids, Journal of Applied Physics **113**, 2013 (011301).
3. A. Dokhan, E.W. Price, J.M. Seitzman, R.K. Sigman, The effects of bimodal aluminum with ultrafine aluminum on the burning rates of solid propellants, Proceedings of the Combustion Institute **29**, 2002 (2939).
4. A. Zygmunt, K. Gańczyk, A. Kasztankiewicz, K. Cieślak, T. Gołofit, Application and properties of aluminum in primary and secondary explosives, Journal of Elementology **22**, 2017 (747).
5. L.T. DeLuca, Overview of Al-based nanoenergetic ingredients for solid rocket propulsion, J.Defence Technology **14**, 2018 (357).

6. F.Wang, Z. Wu, X. Shangguan, Y. Sun, J. Feng, Z. Li, L. Chen, S. Zuo, R. Zhuo and P. Yan, Preparation of Mono-Dispersed, High Energy Release, Core/Shell Structure Al Nanopowders and Their Application in HTPB Propellant as Combustion Enhancers, Scientific Reports **7**, 2017 (1).
7. T.S. Shih, Z.B. Liu, Thermally-Formed Oxide on Aluminum and Magnesium, Materials Transactions **47**, 2006 (1347).
8. L.P.H. Jeurgens, W.G. Sloof, F.D. Tichelaar, E.J. Mittemeijer, Growth Kinetics and Mechanisms of Aluminum-Oxide Films Formed by Thermal Oxidation of Aluminum, Journal of Applied Physics **92**, 2002 (1649).
9. W. Yang, Z.P. Luo, W-K. Bao, H. Xie, Z.S. You, H.J. Jin,Light, strong, and stable nanoporous aluminum with native oxide shell, Science Advances 7, 2021 (28).
10. A.T.M van Gogh, S.J. van der Molen, J.W.J. Kerssemakers, N.J. Koeman, R.P. Griessen, Performance Enhancement of Metal-Hydride Switchable Mirrors Using Pd/ AlOx Composite Cap Layers, Applied Physics Letters. **77**, 2000 (815).
11. K. Gloos, P.J. Koppinen, J.P. Pekola, Properties of Native Ultrathin Aluminium Oxide Tunnel Barriers, Journal of Physics: Condensed Matter **15**, 2003 (1733).
12. A.K. Petford-Long, Y.Q. Ma, A. Cerezo, B.W. Karr,D.J. Larson, E.W. Singleton, The Formation Mechanism of Aluminum Oxide Tunnel Barriers: Three-Dimensional Atom Probe Analysis, Journal of Applied Physics **98**, 2005 (124904).
13. G. Gutiérrez, B. Johansson, Molecular Dynamic Study of Structural Properties of Amorphous Al2O3, Physical Review **B65**, 2002 (104202).
14. E.L. Dreizin, Experimental study of stages in aluminium particle combustion in air, Combustion and Flame **105**, 1996 (541).
15. S. Alavi, J.W. Mintmire, D.L. Thompson, Molecular Dynamics Simulations of the Oxidation of Aluminum Nanoparticles, The Journal of Physical Chemistry **B109**, 2005 (209).
16. M. Aykol, K.A. Persson, Oxidation Protection with Amorphous Surface Oxides: Thermodynamic Insights from Ab Initio Simulations on Aluminum, ACS Applied Materials & Interfaces, **10**, 2018 (3039).
17. A. Rai, K. Park, L. Zhou, M.R. Zachariah, Understanding the mechanism of aluminium nanoparticle oxidation, Combustion Theory and Modelling **10**, 2006 (843).
18. B.J. Henz, T. Hawa, M. Zachariah, Atomistic Simulation of the Aluminum Nanoparticle Oxidation Mechanism, Proceedings of the 48th AIAA Aerospace Sciences Meeting, (2010).
19. Q. Chu, B. Shi, L. Liao, K.H. Luo, N. Wang, C. Huang, Ignition and Oxidation of Core–Shell Al/Al2O3 Nanoparticles in an Oxygen Atmosphere: Insights from Molecular Dynamics Simulation, The Journal of Physical Chemistry C**122**, 2018 (29620).
20. A. Hasnaoui, O. Politano, J.M. Salazar, G. Aral, R.K. Kalia, A. Nakano, P. Vashishta, Molecular Dynamics Simulations of the Nano-Scale Room-Temperature Oxidation of Aluminum Single Crystals, Surface Science **579**, 2005 (47).

21. S. Hasani, M. Panjepour, M. Shamanian ,The Oxidation Mechanism of Pure Aluminum Powder Particles, Oxidation of Metals **78**, 2012 (179).
22. L.P.H Jeurgens, W.G Sloof, F.D. Tichelaar, E.J Mittemeijer, Structure and Morphology of Aluminium-Oxide Films Formed by Thermal Oxidation of Aluminium, Thin Solid Films **418**, 2002 (89).
23. N. Amiri, J.B. Ghasemi, H. Behnejad, Atomistic Insights into the Protection Failure of the Graphene Coating under the Hyperthermal Impacts of Reactive Oxygen Species: ReaxFF-Based Molecular Dynamics Simulations,Applied Surface Science**554**, 2021 (149606).
24. M.J. Kim, J.Nriagu, Oxidation of Arsenite in Groundwater Using Ozone and Oxygen, Science of the Total Environment **247**, 2000 (71).
25. S. Gupta, S. Hannah, C.P. Watson, P. Sutta, R.H. Pedersen, N. Gadegaard, H. Gleskova, Ozone Oxidation Methods for Aluminum Oxide Formation: Application to Low-Voltage Organic Transistors, Organic Electronics **21**, 2015 (132).
26. H.F. Ridgway, B. Mohan, X. Cui, K.J. Chua, M.R. Islam, Molecular Dynamics Simulation of Gas-Phase Ozone Reactions With Sabinene and Benzene, Journal of Molecular Graphics and Modelling **74**, 2017 (241).
27. Z. Lian, C. Zhu, S. Zhang, W. Ma, Q. Zhong, Study on the Synergistic Oxidation of Sulfite Solution by Ozone and Oxygen: Kinetics and Mechanism, Chemical Engineering Science **242**, 2021 (116745).
28. A. Kuznetsova, J.T. Yates, G. Zhou, J.C. Yang, X. Chen, Making a Superior Oxide Corrosion Passivation Layer on Aluminum Using Ozone, Langmuir **17**, 2001 (2146).
29. K. Koike, T. Fukuda, High-Concentration Ozone Generator for Oxidation of Silicon Operating at Atmospheric Pressure, Review of Scientific Instruments. **71**, 2000 (4182).
30. J. Evertsson, F. Bertram, F. Zhang, The Thickness of Native Oxides on Aluminum Alloys and Single Crystals, Applied Surface Science 349, 2015 (826).
31. C. Zhang, K. Abdijalilov, H. Grebel, Surface Enhanced Raman with Anodized Aluminum Oxide Films, Journal of Chemical Physics **127**, 2007 (044701).
32. A.E. Gheribi, S. Poncsak, S. Guérard, J-F Bilodeau, L. Kiss, and P. Chartrand, Thermal conductivity of the sideledge in aluminium electrolysis cells: Experiments and numerical modelling, Journal of Chemical Physics **146**, 2017 (114701).
33. D. Flötotto, Z.M. Wang, L. Jeurgens, E.J. Mittemeijer, Intrinsic Stress Evolution during Amorphous Oxide Film Growth on Al Surfaces, Applied Physics Letters**104**, 2014 (091901).
34. L.S.I. Liyanage, S-G Kim, J. Houze, S. Kim, M. A. Tschopp, M. I. Baskes, and M. F. Horstemeyer,Structural, Elastic, and Thermal Properties of Cementite (Fe3C) Calculated Using a Modified Embedded Atom Method, Physical Review **B89**, 2014 (094102).
35. J. Wei, W. Zhou, S. Li, P. Shen, S. Ren, A. Hu,W. Zhou, Modified Embedded Atom Method Potential for Modeling the Thermodynamic Properties ofHigh Thermal Conductivity Beryllium Oxide, ACS Omega **4**, 2019 (6339).

36. A.C.T. Van Duin, S. Dasgupta, F. Lorant, W.A. Goddard, ReaxFF : A reactive force field for hydrocarbons, Journal of Physical Chemistry A**105**, 2001 (9396).
37. T.P. Senftle, S. Hong, A.C.T. Van Duin, M.d.M. Islam, S.B. Kylasa, Y. Zheng, et al. , The Reaxff Reactive Force-Field: Development, Applications and Future Directions, Computational Materials **2**, 2016 (1).
38. S. Hong, A.C.T. Van Duin, Molecular Dynamics Simulations of the Oxidation of Aluminum Nanoparticles using the ReaxFF Reactive Force Field, Journal of Physical Chemistry C**119**, 2015 (17876).
39. K. Nomura, R. K. Kalia, A. Nakano, RXMD: A Scalable Reactive Molecular Dynamics Simulator for Optimized Time- to-Solution, SoftwareX, **11**, 2020 (100389).
40. A. Rahnamoun, M. Cagri Kaymak, M. Manathunga, A.W. Götz, A.C.T. van Duin, K.M. Merz Jr. and H.M. Aktulga, ReaxFF/AMBER—A Framework for Hybrid Reactive/ Nonreactive Force Field Molecular Dynamics Simulations, Journal of Chemical Theory and Computation, **16**, 2020 (7645).
41. D.V. Ilyin, W.A. Goddard, J. Julius, T. Cheng, First-Principles–Based Reaction Kinetics from Reactive Molecular Dynamics Simulations: Application to Hydrogen Peroxide Decomposition, Proceedings of the National Academy of Sciences of the USA **116**, 2019 (18202).
42. W.J. Mortier, S.K. Ghosh, S. Shankar, Electronegativity-Equalization Method for the Calculation of Atomic Charges in Molecules, Journal of the American Chemical Society **108**, 1986 (4315).
43. N. Amiri, H. Behnejad,Oxidation of Nickel Surfaces through the Energetic Impacts of Oxygen Molecules: Reactive Molecular Dynamics Simulationsn,Journal of Chemical Physics **144**, 2016 (144705).
44. S.J. Plimpton, Fast Parallel Algorithms for Short- Range Molecular Dynamics, Journal of Computational Physics **117**, 1995 (1).
45. A. Stukowski, Visualization and Analysis of Atomistic Simulation Data with OVITO–the Open Visualization Tool, Modell. Simul. Mater. Sci. Eng. **18**, 2009 (015012).
46. W. Humphrey, A. Dalke, K. Schulten,Vmd: Visual Molecular Dynamics, Journal of Molecular Graphics **14**, 1996 (33).
47. M.E. Trybula, P.A. Korzhavyi, Temperature Dependency of Structure and Order Evolution in 2D Confined Oxide Films Grown on Al Substrates Using Reactive Molecular Dynamics, Vacuum **190**, 2021 (110243).
48. M.E. Trybula, P.A. Korzhavyi, Atomistic Simulations of Al(100) and Al(111) Surface Oxidation: Chemical and Topological Aspects of Oxide Structure, Journal of Physical Chemistry C**123**, 2019 (334).
49. K.M.Ø. Jensen, Characterization ofNanomaterials with Total Scattering and Pair Distribution Function Analysis: Examples from Metal Oxide Nanochemistry, CHIMIA **75**, 2021 (368).
50. G. Gutie´rrez, C. Johansson, Molecular Dynamics Study of Structural Properties of Amorphous Al2O3, Physical Review **B65**, 2002 (104202).

51. G.Gutie´rrez, A.B. Belonoshko, R. Ahuja, B. Johansson, Structural Properties of Liquid Al2O3: A Molecular Dynamics Study, Physical Review **E61**, 2000 (2723).
52. L. Gang, N. Liangliang, H. Weizhe, L. Yu, Z. Chaoyang,Atomistic Insight into the Microexplosion-Accelerated Oxidation Process of Molten Aluminum Nanoparticles, Combustion and Flame **214**, 2020 (238).
53. S.K.R.S. Sankaranarayanan, E. Kaxiras, S. Ramanathan, Atomistic Simulation ofField Enhanced Oxidation of Al (100) Beyond the Mott Potential, Physical Review Letters, **102**, 2009 (0955041).
54. A. Hasnaoui, O. Politano, J.M. Salazar, G. Aral, Nanoscale Oxide Growth on Al Single Crystals at Low Temperatures: Variable Charge Molecular Dynamics Simulation, Physical Review **B73**, 2003 (035427).
55. A. Perron, S. Garruchet, O. Politano, G. Aral, V. Vignal, Oxidation of Nanocrystalline Aluminum by Variable Charge Molecular Dynamics, Journal Physics and Chemistry of Solids **71**, 2010 (119).
56. L. Chen, H. Luo, Z. Li, A. Sha, Effect of Al Doping on the Early-Stage Oxidation ofNi-Al Alloys: A ReaxFF Molecular Dynamics Study, Applied Surface Science **563**, 2021 (150097).
57. A. Kazor, I.W. Boyd, Ozone-Induced Rapid Low Temperature Oxidation of Silicon, Journal of Applied Physics Letters **63**, 1993 (2517).
58. Y.Li, R.K. Kalia, A. Nakano, P. Vashishta, Size Effect on the Oxidation of Aluminum Nanoparticle: Multimillion-Atom Reactive Molecular Dynamics Simulations, Journal of Applied Physics **114**, 2013 (134312).
59. T.V. Larson, N.R. Horike, H. Harrison, Oxidation of Sulfur Dioxide by Oxygen and Ozone in Aqueous Solution: A kinetic study with significance to atmospheric rate processes, Atmospheric Environment **12**, 1977 (1597).
60. M.J. Cyster, J.S. Smith , N. Vogt, G. Opletal, S.P. Russo, J.H. Cole, Simulating the Fabrication of Aluminium Oxide Tunnel Junctions, Quantum Information **7,** 2021 (1).

Figures

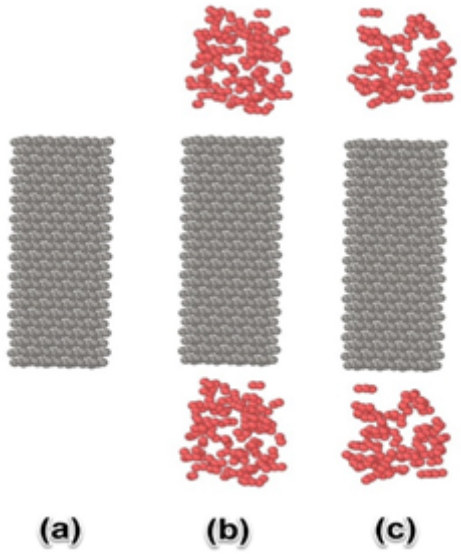

Figure 1

Initial configuration Al(100): (a) 576 Al atoms; (b) Al atoms with 150 oxygen molecules; (c) Al atoms with 100 ozone molecules: Grey color stands for aluminum atoms, and the red color stands for oxygen atoms.

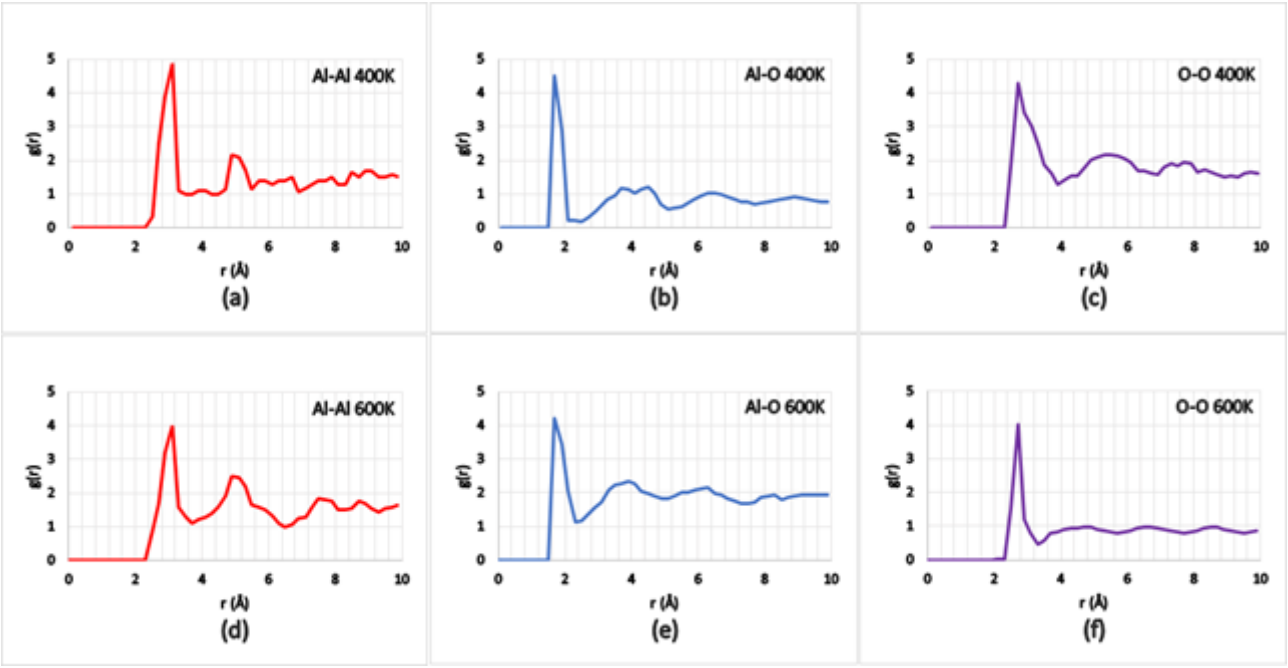

Figure 2

Radial distribution function Al / O_2 of (a,d) Al-Al; (b,e) Al-O; (c,f) O-O; (a,b,c) at 400 K; (d,e,f) at 600 K; gas density:0.47 g/cm^3.

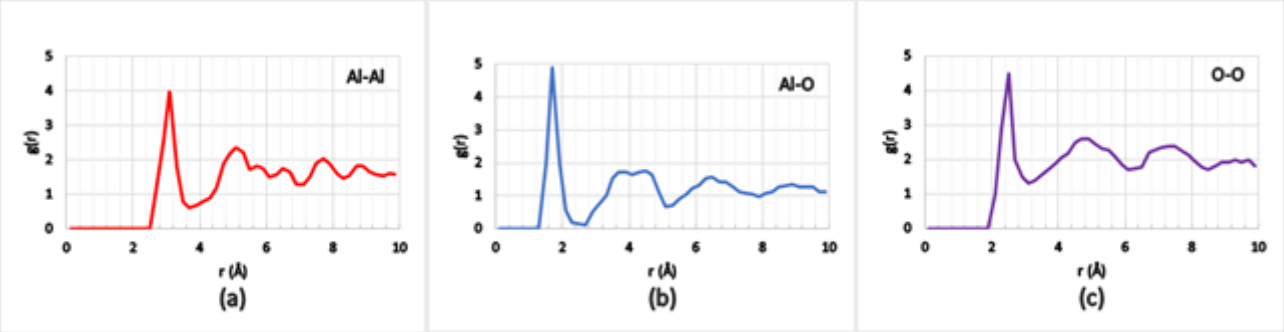

Figure 3

Radial distribution function Al / O_3 of (a) Al-Al; (b) Al-O; (c) O-O at 600 K and initial ozone gas density:0.47 g/cm^3.

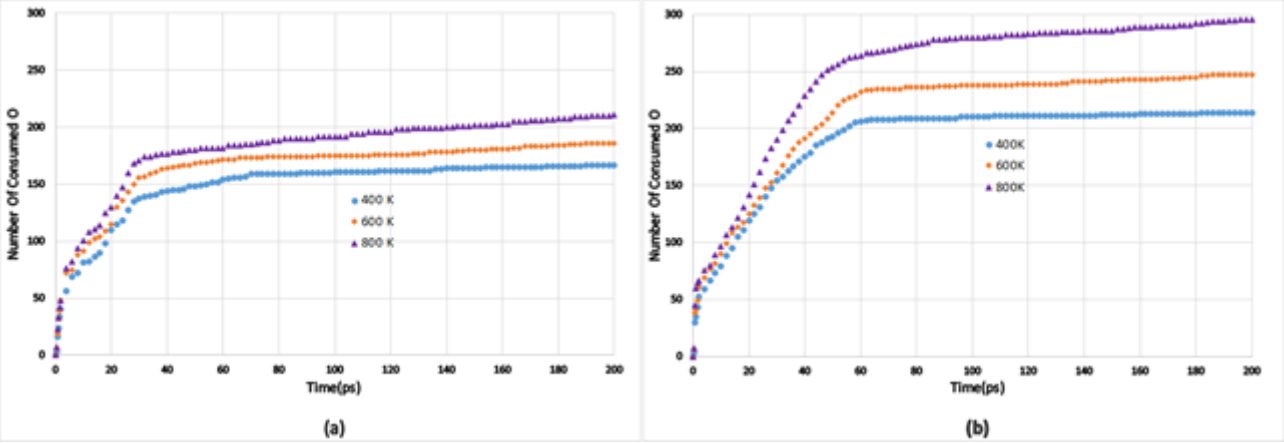

Figure 4

The amount of O-atom consumption as a function of time at divergent temperatures: (a) Al-oxygen; (b) Al-ozone.

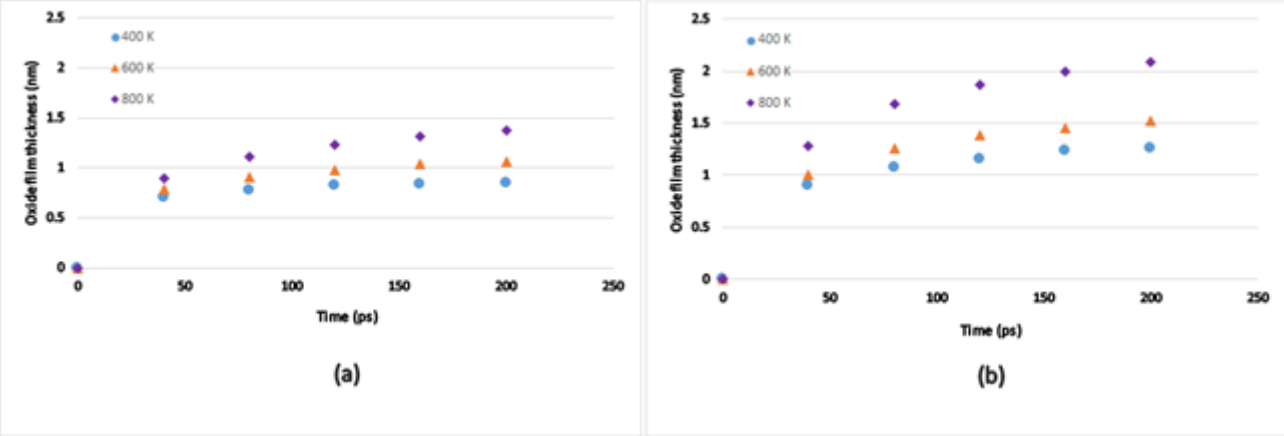

Figure 5

Calculated thickness of oxide films formed on Al(100): (a) with oxygen at 400, 600, and 800 K; (b) with ozone at 400, 600, and 800 K.

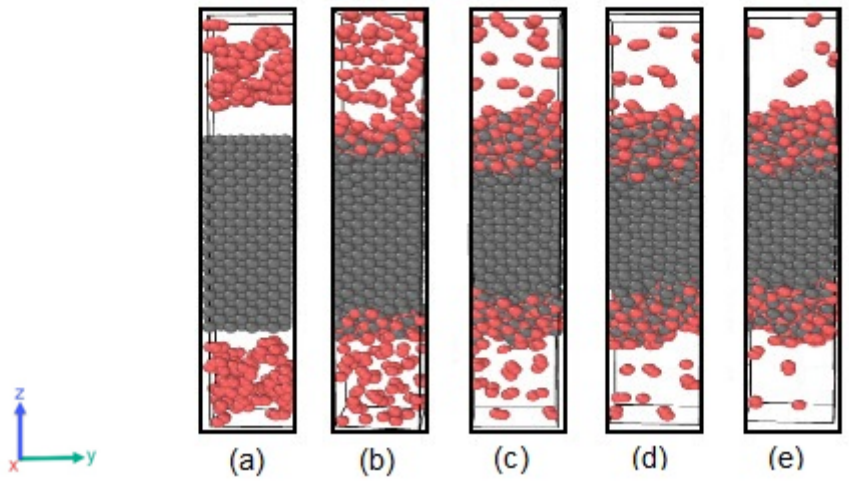

Figure 6

Front view snapshots of the oxide film in Al/O_3 with the passage of time at 600 K: (a) t=0 ps; (b) t=50 ps; (c) t=100 ps; (d) t=150 ps; (e) t=200 ps. Grey color stands for an aluminum atom and the red color stands for an ozone molecule.

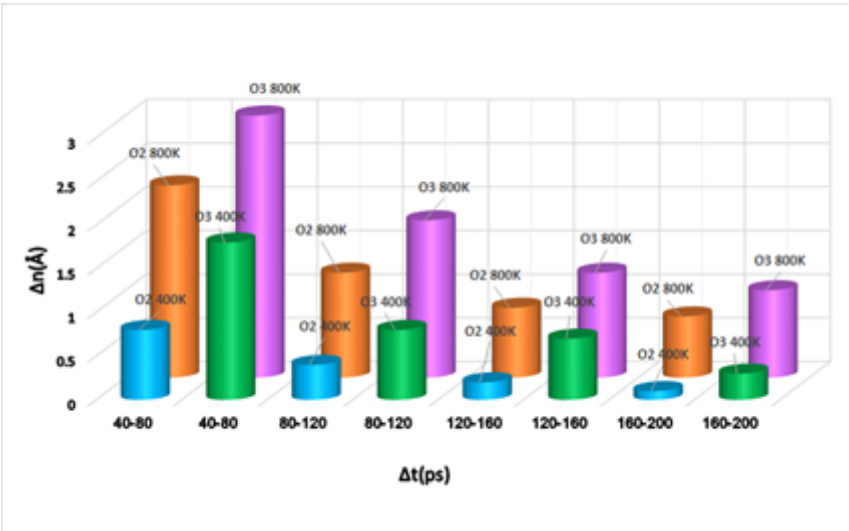

Figure 7

The average layer-growth rate for Al-ozone, and Al-oxygen at 400, and 800 K.

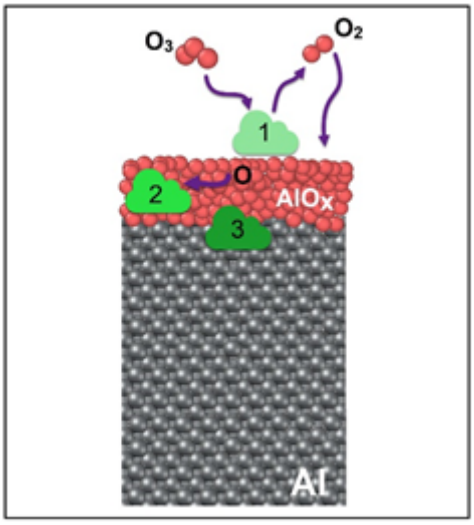

Figure 8

Graphical view of aluminum oxidation with ozone: 1) ozone molecules striking and generating radicals; 2) Diffusion of radicals in aluminum; 3) concatenation of oxygen atoms at the oxide-metal interface.

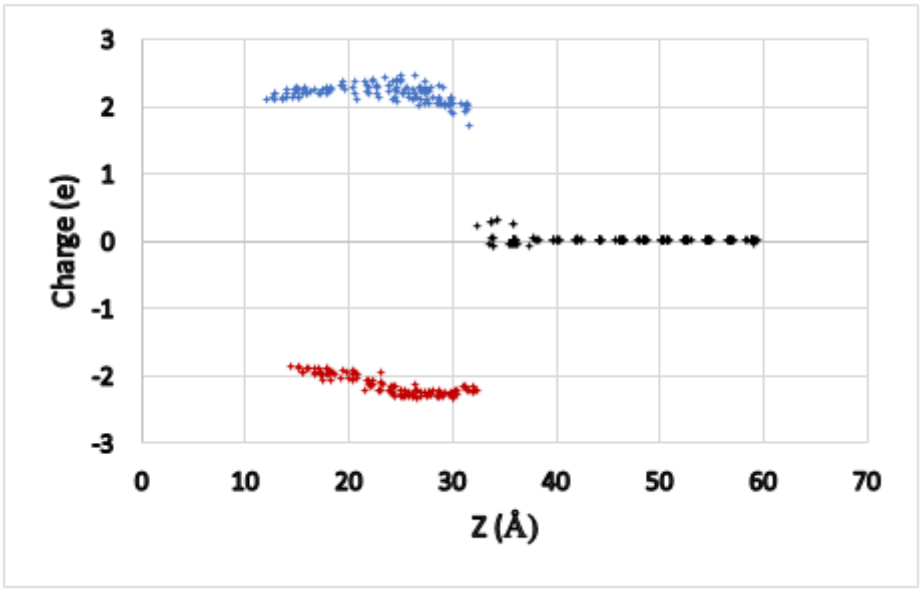

Figure 9

Charge distribution for oxygen and aluminum atoms in Al-O_3 system as a function of z- axis. The blue color represents charge distribution for aluminum atoms and the red color represents charge distribution for oxygen.